# A TIME-FREQUENCY POST-PROCESSING TECHNIQUE FOR THE CHARACTERIZATION OF THE UNSTEADY PHENOMENA IN THE TURBOMACHINES

G. Pavesi G. Cavazzini G. Ardizzon

Department of Mechanical Engineering, University of Padova, Italy
giorgio.pavesi@unipd.it giovanna.cavazzini@unipd.it guido.ardizzon@unipd.it

## ABSTRACT

This paper presented a data processing technique that combines different signal analyses for the spectral characterization of the unsteady phenomena developing in the turbomachines. Tools of the classical Fourier analysis, such as second order spectra, were combined with tools of the time-frequency analysis (wavelets, cross-wavelet, coherence wavelet functions) to identify unsteady phenomena, to define their spectral structure, to analyse their evolution in time and to determine their possible propagation direction and velocity.

Because of the non-linearity of several unsteady phenomena developing in turbomachines, high-order moment functions were applied to discriminate between non-linearly coupled pulsations and self-excited pulsations and to determine the fraction of the power of each pulsation that was due to the non-linear interaction of unsteady phenomena.

## INTRODUCTION

In past years several analytical and experimental approaches were carried out to study the unsteady phenomena that occur in turbomachines. The resulting velocity fluctuations were tracked in continuously running facilities thanks to LDV and PIV, and experiments were conducted to measure the pressure fluctuations. In order to study more in depth the characteristics of these phenomena, spectral analyses were also considered by researchers and linear analysis techniques, such as auto- and cross-power spectra, were applied to study the spectral structure.

Although this linear spectral approach allows finding and analyzing the spectral components contained in the measured signals, it does not provide information about their time evolution and about possible interaction mechanisms that could generate non-linearly coupled pulsations. In order to investigate these aspects second and higher order analyses should be used [1,2,3,4,5,6].

The post-processing analysis presented in this paper combines the linear spectral analysis techniques with the most advanced time-frequency techniques in order to identify and characterize the spectral structure and the evolution in time of the unsteady phenomena developing in the turbomachines. For a thorough investigation of the non-linear aspects of these phenomena, high-order spectral techniques are also presented.

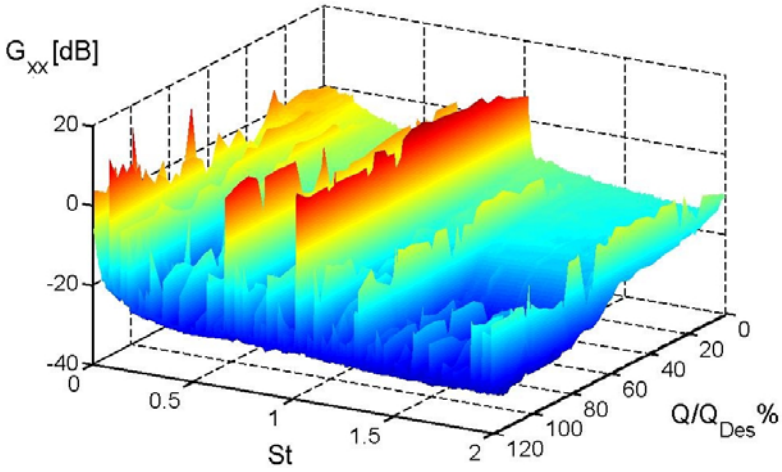


**Fig. 1: Power Spectrum of the unsteady pressure, measured by a micro-transducer in the diffuser blade, versus the flow rate and the St (n=600 rpm)**

## RESULTS AND DISCUSSION

The proposed signal post-processing technique was applied to unsteady pressure measurements, carried out by micro pressure transducers at the impeller inlet and outlet and in the diffuser blades of a centrifugal pump.

The power spectra of the acquired pressure signals allowed to identify the main spectral components of the signals (fig. 1). Besides the blade passage frequency and its harmonics, there were several peaks identifiable in the spectrum and it was difficult to discriminate between self-excited pulsations and eventually coupled pulsations due to

non-linear phenomena interaction.
The higher order spectral analysis allows to distinguish between spontaneously excited modes and coupled modes, and hence to identify the self-excited peaks that dominates the spectra. In particular, the third order spectrum of a signal x(t), known as "bispectrum" and determined as:

$$B(k,l) = E[\, X_k X_l X^*_{k+l} \,] \tag{2.1}$$

where X is the Fourier Transform of the signal x(t), X* denotes its complex conjugate and k and l are frequency indexes [1,2,7,8,9] allows to measure the nonlinear dependence between three spectral components (k,l,k+l). It has non-zero value when the three components are nonlinearly coupled.

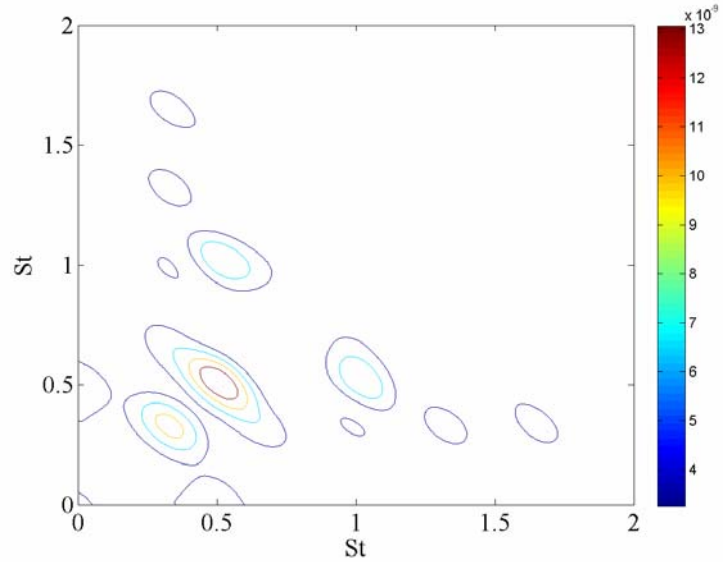


**Fig. 2 Bispectrum of the unsteady pressure, measured by a micro transducers in the diffuser blade versus the Strouhal number St (n=600 rpm)**

The bispectral analysis of the pressure signals identified the main spectral components ($St_F$=0.664 and $St_S$=0.071), interacting both with each other and with the BPF (fig. 2). All other peaks in the spectra are demonstrated to be harmonics of these fluctuations or non-linear components, generated by the interaction between the pulsating phenomena.

The analysis pointed out the sensitivity of the "bispectrum" at the number of "cumulant" lags used to identify the components nonlinearly coupled. Accurate analysis was obtained adopting a standard upper range equal to the 10% of the number of sample (upper order equal to 820) but with a limited usability. On the other hand the reduction of the number of "cumulant" lags below to 40 reduced the possibility of distinguishing the main spectral components interacting. Probably a sensitivity analysis has to be carried out to highlight the influence of the number of "cumulant" lags to be computed on a good compromise between data accuracy and usability.

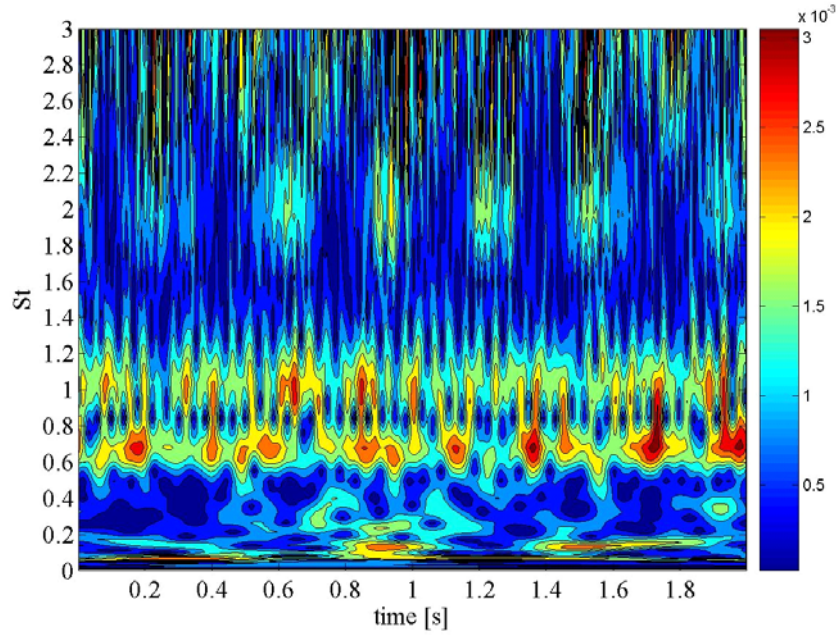


**Fig. 3a Wavelet transform magnitude |Wn| for $Q/Q_{des}$=80%.**

Once identified the dominating frequencies in the pressure signals, their time-evolution was studied by a time-frequency analysis. The wavelet transforms of the pressure signals identify the spectral components constantly present in the spectra and those appearing only in a definite period of time (figs 3a and 3b).

These wavelet transform W(s, n) can be computed via the FFT-based fast convolution:

$$W(s,n) = \sum_{k=0}^{N-1} X_k \left( \sqrt{\frac{2\pi s}{\delta t}} \Psi_0^* (s\omega_k) e^{i\omega_k n \delta t} \right) \tag{2.2}$$

where $X_k$ is the Discrete Fourier Transform (DFT) of $x_n$, k is the frequency index, N is the data series length, s is the wavelet scale, δt is the sampling interval, n is the localized time index, $\Psi_0^*(s\,\omega_k)$ is the complex conjugate of

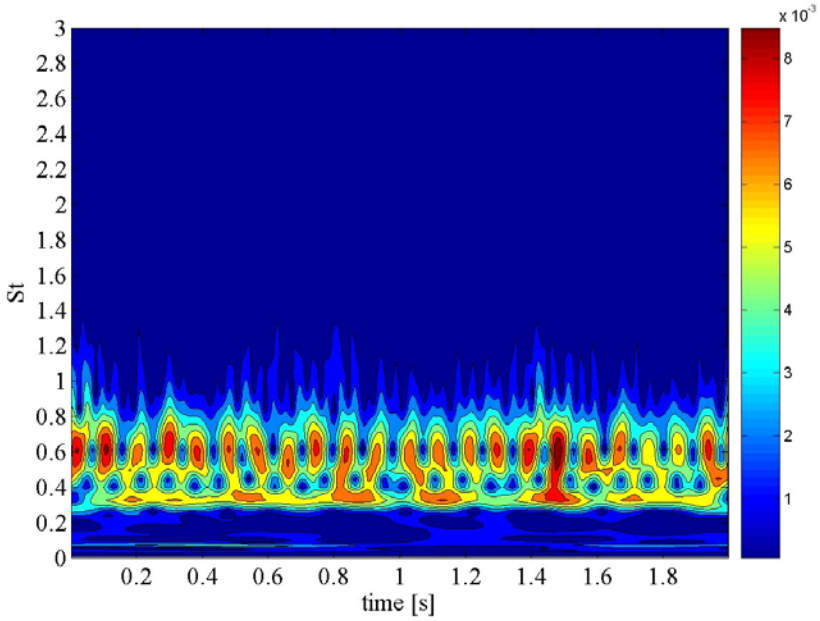


**Fig. 3b Wavelet transform magnitude |Wn| for $Q/Q_{des}$=100%.**

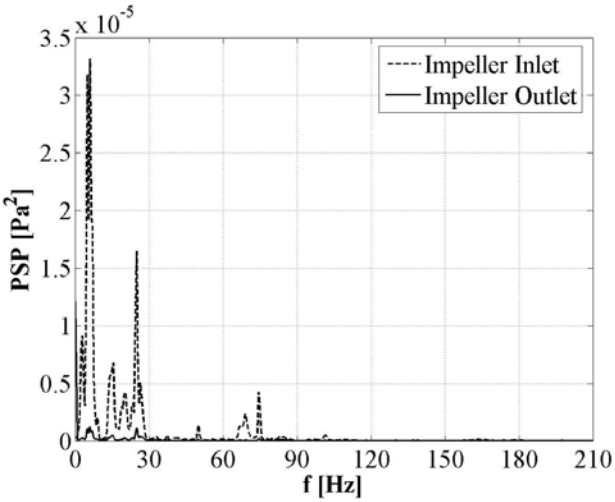


**Fig. 4 Power spectrum of the pressure measured at the impeller inlet and outlet with the pump not-running.**

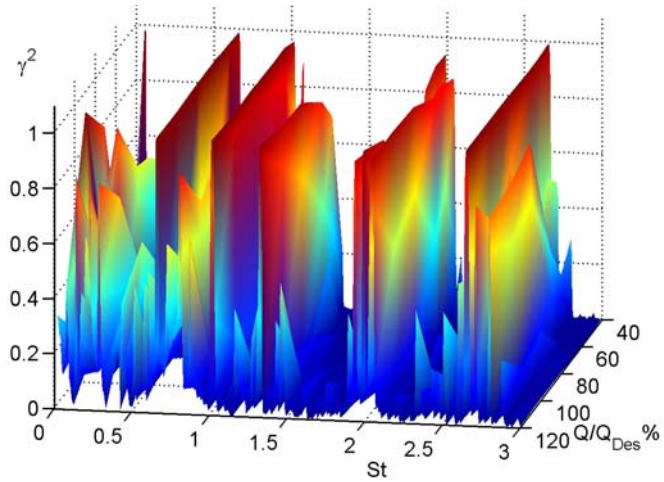


**Fig. 5 Coherence level between micro-transducers placed at the same radial distance at the impeller discharge**

the Fourier transform of the scaled version of the "mother wavelet" $\psi(t)$, $\omega_k$ is the angular frequency (if $k \leq N/2$, $\omega_k = 2\pi k/Ndt$; else $\omega_k = -2\pi k/N\delta t$). Several well-defined mother wavelet functions, such as Paul, DOGs (derivatives of the Gaussian), Mexican Hat and Morlet wavelet, are available for a time-frequency analysis, and the choice depends on several factors, according to the expected characteristics of the analyzed phenomena and on the information that have to be extracted [10]. The Paul and Morlet wavelets are complex functions and allow to extract information about both amplitude and phase, whereas the DOGs and the Mexican Hat are real valued functions, returning only a single component with a very high resolution in time but a low resolution in frequency. Moreover, when the investigated phenomena are expected to have continuous variations in time for the wavelet amplitude, non-orthogonal wavelets functions, such as Morlet, Paul and DOGs, have to be preferred, whereas orthogonal wavelets (Mexican Hat, Haar,…) are more suitable for wavelet spectrum highly correlated in time.

In this case, the Morlet wavelet was chosen with the wavenumber $2\pi f_0=6$ since it provided a good balance between time and frequency localization.

The combined analysis in the frequency and time-frequency domains of the pressure signals acquired at different positions of the impeller and diffusers, allowed to discriminate between system fluctuations and fluid-dynamical fluctuations, to determine the zone of greater intensity of these fluctuations in the pump and to define their evolution in time. In this case, it was evident an unsteadiness in time of the pulsations at St=0.664, demonstrated to have a fluid-dynamical origin, because of their absence in the spectra of the not-running pump (fig. 4) and in the spectra of the system vibrations.

To evaluate the possible direction and velocity of propagation of the identified pulsating phenomena, the pressure signals acquired by transducers placed at different positions can be compared both in the frequency and in the time frequency domains.

The cross-spectra of two sampled pressure signals $x_n$ and $y_n$:

$$G^{xy}(f) = \frac{1}{NW_H}\sum_{k=1}^{N}\left[X_k^*(f)Y_k(f)\right] \qquad (2.3)$$

(where N is the number of samples segments, $W_H$ is weighting constant corresponding to the time window chosen, $X_k(f)$ and $Y_k(f)$ are the fast

Fourier transform of the k[th] data segment and $X_k(f)^*$ is its complex conjugate), and the coherence function between the two signals:

$$\gamma^2(f) = \frac{\left|G^{xy}(f)\right|^2}{G^{xx}(f)\cdot G^{yy}(f)} \tag{2.4}$$

allow to verify the propagation of the identified phenomena. High levels of the coherence function (fig. 5) between pressure transducers placed at different azimuthal or radial positions at the impeller discharge demonstrated a propagation of the pulsating phenomena at St=0.664 both in the circumferential and radial direction.

Moreover, the phase information obtained by the cross-correlation analysis, also allowed to determine the propagation velocity. The angular rotation velocity of the identified pulsating structure $\omega_p$ at St=0.664, normalized by the angular impeller rotation speed ω, was calculated by:

$$\frac{\omega_p}{\omega} = \frac{f\Delta\theta}{\gamma_p}60\frac{360}{2\pi n} = \frac{\Delta\vartheta}{\tau}\frac{60}{2\pi n} \tag{2.5}$$

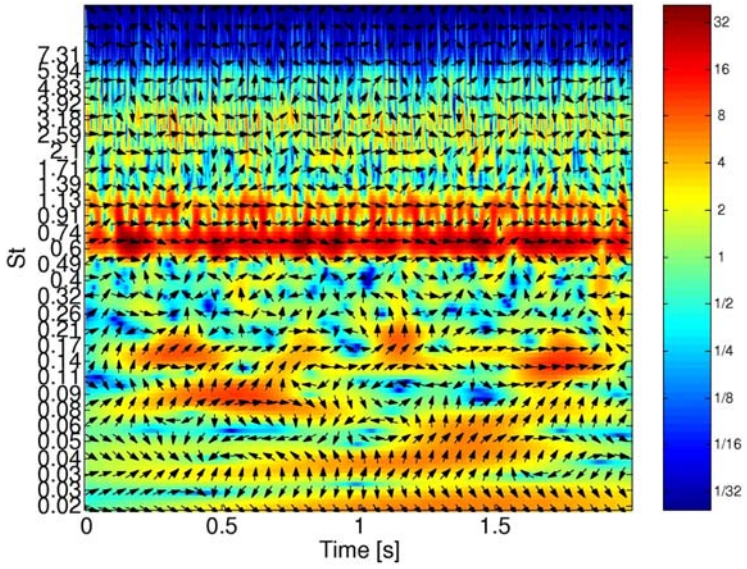


**Fig. 6 Cross-wavelet transform between pressure transducers placed at the impeller discharge ($Q/Q_{des}$=50%)**

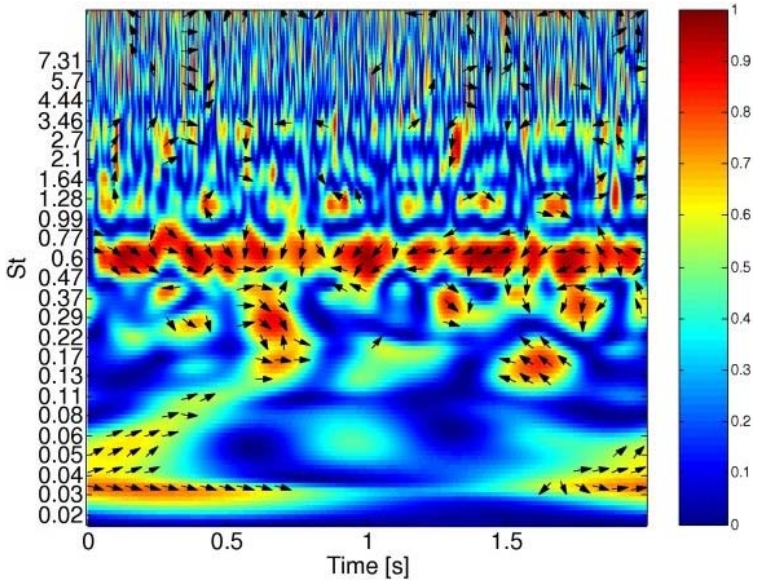


**Fig. 7 Wavelet coherence between pressure transducers placed at the impeller discharge at different radial positions ($Q/Q_{des}$=40%)**

where the time delay τ, the angular distance between the transducers Δθ and the impeller rotation speed n were known.

Whereas the radial propagation velocity $C_{rp}$ of the identified structure downstream of the impeller was calculated by:

$$\frac{C_{rp}}{U_2} = \frac{f\Delta R}{\gamma_p}60\frac{360}{2\pi n}\frac{1}{R_2} = \frac{\Delta R}{\tau}\frac{60}{2\pi n}\frac{1}{R_2} \tag{2.6}$$

where $R_2$ and $U_2$ are respectively the radius and the peripheral velocity at the impeller blade trailing edge, and $\Delta R$ is the radial distance between the transducers.

The continuity in time of this propagation was verified in the time-frequency domains by means of the cross-wavelet function, defined by Li in 1998 [11], whose corresponding cross-wavelet spectrum for two sampled signals $x_n$ and $y_n$ can be determined as:

$$W^{xy}(s,n) = W^x(s,n)W^{y*}(s,n) \tag{2.7}$$

where $W^x(s,n)$ and $W^y(s,n)$ are the wavelet transforms of the signals and W* states for the complex conjugate [12, 13]. In fig. 6 the high and time-independent level of the cross-wavelet spectrum for the frequency at St=0.664 combined with a time-independent phase coincidence between the two signals at St=0.664 highlights a time-independent propagation of the phenomenon in the circumferential direction with a

constant rotation velocity. The in-phase relation was presented as arrows pointing right, the anti-phase relation as arrows pointing left, the 90° phase displacement as arrows pointing straight on.

Furthermore, the wavelet coherence allows to measure the coherence between two sampled signals not only in the frequency domain but also in time domain:

$$R_n^2(s) = \frac{\left|\left\langle W^{xy}(s,n)\right\rangle\right|^2}{\left\langle\left|W^x(s,n)\right|^2\right\rangle \cdot \left\langle\left|W^y(s,n)\right|^2\right\rangle} \tag{2.8}$$

where $\langle\cdot\rangle$ indicates a smoothing, done using a weighted running convolution in both the time and scale directions. The time smoothing is obtained with a filter corresponding to the absolute value of the wavelet function at each scale, normalized to have a total weight of unity, whereas the scale smoothing is done using a boxcar filter of width $\delta j_0$, whose value is empirically determined. In the numerator, the real and imaginary parts of the cross-wavelet spectrum are smoothed before the absolute value is calculated, whereas in the denominator the smoothing is done on the square wavelet power spectra of the two signals. The amount of the smoothing depends on the mother wavelet and on the scale [12,14,15]. For the complex Morlet wavelet function, the filter for the time smoothing is a Gaussian $exp(-t^2/(2s)^2)$, whereas $\delta j_0$ is equal to 0.6.

In fig. 7, a time-independent coherence for the frequency at St=0.664 between transducers placed at different radial positions demonstrates a coherent propagation of the phenomenon not only in the circumferential direction but also in the radial direction.

## REFERENCES

[1] Knisely C., Rockwell D, (1982): "Self-sustained low-frequency components in an impinging shear layer", Journal of Fluid Mechanics, vol. 116, pp. 157-186.

[2] Akin O., Rockwell D. (1994): "Actively Controlled Radial Flow Pumping System: Manipulation of Spectral Content of Wakes and Wake-Blade Interactions", ASME, Journal of Fluids Engineering, vol. 116, pp. 528-537

[3] Kim Y.C., Powers E.J. (1979): "Digital Bispectral Analysis and Its Applications to Nonlinear Wave Interactions", IEEE Transactions on Plasma Science, vol. PS-7, n. 2. June 1979

[4] Kim Y.C., Beall J.M., Powers E.J., Miksad R.W. (1980): "Bispectrum and nonlinear wave coupling", Phys. Fluids, vol. 23, pp. 258-263

[5] Hasselmann K., Munk W.H., MacDonald G.J.F. (1963): "Bispectra of ocean waves", Time Series Analysis, pp.125-139, Wiley

[6] Lii K.S., Rosenblatt M., Van Atta C. (1976): "Bispectral measurements in turbulence", Journal of Fluid Mechanics, vol. 77, pp.45-62.

[7] Rosenblatt M., Van Ness J.W. (1965): "Estimation of the Bispectrum", Ann. Math. Stat., vol. 36, pp-1120-1136.

[8] Nikias C.L., Mendel J.M. (1993): "Signal processing with high-order spectra", IEEE Signal Processing Magazine, vol. 10, n. 3, pp.10-37, July 1993

[9] Nikias C.L., Petropulu A.P.: "High-Order Spectral Analysis: A non-linear Signal Processing Framework", New Jersey: Prentice Hall, 1993

[10] Farge M. (1992): "Wavelet transforms and their application to turbulence", Annual Review of Fluid Mechanics, vol. 24, pp. 395-457

[11] Li H. (1998): "Identification of rotating pressure waves in a centrifugal compressor diffuser by means of the wavelet cross-correlation", Int. J. Wavelets, Multiresolution Inf. Processes, vol. 4, no. 2, pp. 373-382

[12] Torrence C., Compo G. (1998): "A Practical Guide to Wavelet Analysis", Bulletin of the American Meteorological Society, vol. 79, no.1, p. 61-78, January 1998

[13] Grinstead A., Moore J.C., Jevrejeva S. (2004): "Application of the cross-wavelet transform and wavelet coherence to geophysical time series", Nonlinear Processes in Geophysics, vol. 11, p. 561-566

[14] Torrence C., Webster P.J. (1999): "Interdecadal changes in the ensomonsoon system", J. Clim., vol. 12, pp. 2679-1690.

[15] Grinsted A. : Crosswavelet and wavelet coherence software, private communication.